Available online at www.sciencedirect.com
SCIENCE DIRECT®
International Journal of Mechanical Sciences 45 (2003) 1913–1927
International Journal of MECHANICAL SCIENCES
www.elsevier.com/locate/ijmecsci

# Investigation of the friction effect at pin joints for the five-point double-toggle clamping mechanisms of injection molding machines

Wen Yi Lin[a], Kuo Mo Hsiao[b,*]

[a] *Department of Mechanical Engineering, De Lin Institute of Technology, 1 Alley 380, Ching Yun Road, Tucheng, Taiwan, ROC*

[b] *Department of Mechanical Engineering, National Chiao Tung University, 1001 Ta Hsueh Road, Hsinchu, Taiwan, ROC*

Received 7 September 2002; received in revised form 9 October 2003; accepted 5 November 2003

**Abstract**

In this study, an analytical formulation for the necessary thrust of the crosshead of the five-point double-toggle clamping mechanism during real-mold clamping operation is proposed in order to investigate the effect of the friction at pin joints. The friction is considered to be a Coulomb friction. The inertia effects are not considered.

Numerical examples are studied for different values of coefficient of friction to investigate the effects of friction at pin joints. In order to estimate the kinetic friction coefficient at pin joints, the motor torques required for real-mold clamping obtained by the present study are adjusted by using different values of coefficient of friction and mechanical efficiency to fit the experimental data.


*Keywords:* Five-point double-toggle clamping mechanism; Injection molding machines; Coulomb friction

## 1. Introduction

The five-point double-toggle mold-clamping mechanism, as shown in Fig. 1, is most extensively used for injection molding machines with clamping force between 50 and 500 metric tons, because of the ideal kinematic velocity feature and mechanical advantage [1,2]. In recent years, injection molding machines of this type with clamping force up to 5000 metric tons have been developed.

* Corresponding author. Fax: +886-35-720-634.
*E-mail address:* kmhsiao@cc.nctu.edu.tw (K. Mo Hsiao).

0020-7403/$ - see front matter © 2003 Elsevier Ltd. All rights reserved.
doi:10.1016/j.ijmecsci.2003.10.010

**Nomenclature**

| | |
|---|---|
| $a, b, c, k_i$ $(i = 1–4)$ | parameters defined in Eq. (27) |
| $A_1, A_2, A_c$ | cross-sectional areas of link 1, link 2, and the tie bar |
| $d_A$ | vertical distance between point $C$ and point $A$ |
| $d_E$ | vertical distance between point $C$ and point $E$ |
| $E_1, E_2, E_c$ | Young's Modulus of link 1, link 2, and the tie bar |
| $F_{ij}, M_{ij}$ $(i, j = 1–6)$ | forces and moments exerted by all members $i$ on a single member $j$ |
| $F_{AB}, F_{BF}, F_{CF}$ | axial forces in a single link 1, the segments $BF$ and $CF$ of a single link 2 |
| $F_0$ | thrust applied to the crosshead |
| $F_{0,\max}$ | maximum value of the thrust $F_0$ during real-mold clamping process |
| $F_{cl}$ | clamping force |
| $L_i$ $(i = 1–4)$ | distances between points $A$ and $B$, $B$ and $C$, $D$ and $E$, and $C$ and $D$ |
| $L_{CF}$ | distance between points $C$ and $F$ |
| $L_c$ | length of the tie bar |
| $n_i$ $(i = 1–4)$ | the number of member $i$ |
| $n_c$ | the number of the tie bar |
| $r_B, r_C, r_D$ | radii of pin joints $B$, $C$, and $D$ |
| $S_C$ | displacement of the tailstock platen defined in Eq. (6) |
| $\bar{S}_C$ | parameter defined in Eq. (7) |
| $U_E$ | the horizontal displacement of the crosshead |
| $\alpha, \beta, \gamma, \gamma_C, \phi$ | angles defined in Figs. 2 and 3 |
| $\alpha_C, \beta_C, \phi_C$ | angles $\alpha, \beta$ and $\phi$ in the position when the moving mold is just in contact with the stationary mold |
| $\beta_\mu, \phi_\mu$ | angles defined in Fig. 3 |
| $\delta_{AB}, \delta_{BC}, \delta_{DE}$ | axial shortened lengths of links 1, 2 and the crosshead link |
| $\delta_{BF}, \delta_{CF}$ | shortened lengths of axial segments $BF$ and $CF$ of links 2 |
| $\mu$ | coefficient of friction |
| $\rho_B, \rho_C, \rho_D$ | friction radii of pin joints $B$, $C$, and D |
| $(\sim)$ | quantity in the state of the final position of mold clamping process |

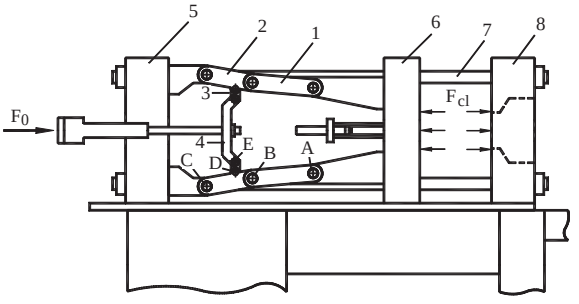


Fig. 1. Five-point double-toggle clamping mechanism of the injection molding machine.

It is well known that the ideal mechanical advantage becomes infinity for the toggle clamping mechanism free from the action of friction at pin joints when the toggle is fully extended in a straight line. However, in practice, the existence of friction at pin joints diminishes the mechanical advantage. The necessary input force for selecting the size of the clamping cylinder or servo electric motor should be directly based on the necessary thrust of the crosshead, rather than the mechanical advantage. To determine the mechanical advantage and the further necessary thrust applied to the crosshead during real-mold clamping operation, the deformations of the tie bars and toggle linkage, and the friction at pin joints should be taken into account [3]. If the necessary thrust of the crosshead cannot be determined correctly, the clamping cylinder diameters or rated output capacities of clamping servo electric motors may be overestimated or underestimated. Furthermore, the accuracy for the prediction of the clamping force from the control of the machine's central mold adjustment system may be affected if the correct value of friction coefficient at pin joints cannot be determined. However, to the authors' knowledge, the coefficient of friction and the effect of friction at pin joints on toggle clamping mechanisms have not been reported in the literature. The aim of this paper is to investigate the effect of friction and to estimate the friction coefficient at pin joints for the mold clamping operation. An elasto-static model for the necessary thrust of the crosshead of the five-point double-toggle clamping mechanism during mold clamping operation is proposed to investigate the effect of friction at pin joints. On the other hand, the estimation of the friction coefficient at pin joints is presented by the comparison between the motor torques required for mold clamping operation under different friction coefficients obtained by the present study and those obtained by experiments.

Lubrication of the joints is crucial to the satisfactory operation of the toggle clamping mechanism [2]. Hydrodynamic lubrication between toggle pins and bushings cannot be achieved due to the reciprocating motion of the toggle mechanism and heavy contact forces. The lubrication between the two members may be considered as boundary or thin-film lubrication [4]. A partial breakdown of a thin oil or grease film between the two members usually occurs during real-mold clamping, because of heavy forces. Such situation may cause direct physical contact and rubbing between two metal members. This type of friction may be considered as dry or Coulomb friction at a journal bearing [5]. Conservatively, it may be reasonable to assume that Coulomb friction at pin joints is valid for mold clamping operation [3]. Thus, Coulomb friction is used in this study.

## 2. Analysis of the toggle clamping system under real-mold clamping

Let members 1–8 shown in Fig. 1 denote moving-platen-side links (1), tailstock-platen-side links (2), crosshead links (3), crosshead (4), tailstock platen (5), moving platen (6), tiebars (7), and stationary platen (8), respectively, for a toggle clamping system throughout this study. Points $A$ to $E$ denote centers of pin joints. The moving platen and the tailstock platen are linked together by a set of toggle linkages that are driven by the thrust transmitted from the clamping cylinder or servo electric motor to the crosshead so that the moving platen can move forward to the right for molding clamping function. During the mold clamping operation, the tailstock platen will move to the left and the tiebars will be stretched after the contact between the moving platen (mold) and the stationary platen (mold). This part of mold clamping operation is called real-mold clamping in this paper. In the process of real-mold clamping, in order to develop the clamping force, the toggle

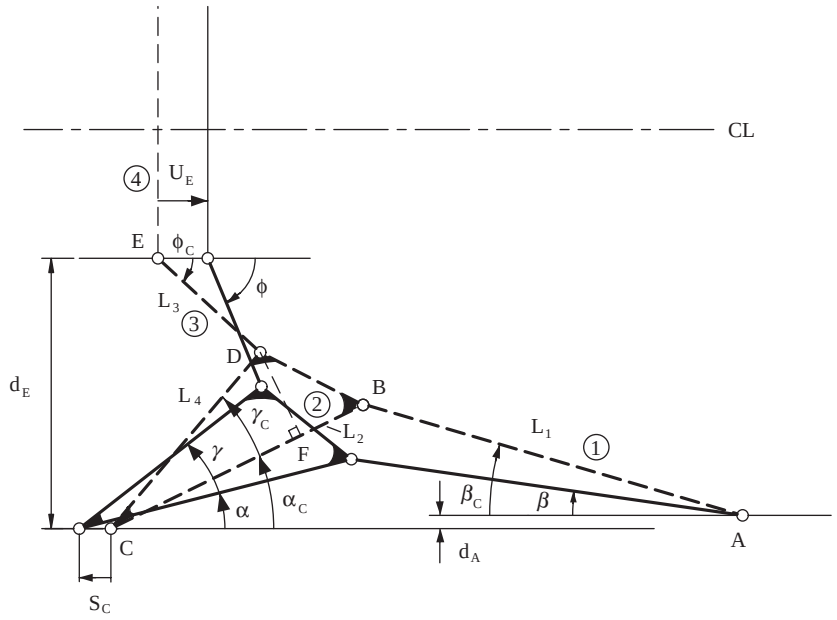


Fig. 2. Geometry of the toggle linkage during real-mold clamping.

clamping mechanism must overcome the friction forces at pin joints and slider connections, and the total deformation force of the tiebars. Here, the slider connections comprise the crosshead and the guiderods, and the tailstock platen and the precision ground steel bands. The effect of the toggle linkage deformation should be considered unless the stiffness of the toggle linkage is much greater than that of the tiebars. In this paper, only the real-mold clamping operation is considered, and the following assumptions are made:

(1) The axial deformation displacements of links and tiebars are small, and the flexural deformations of links and tiebars are negligible.
(2) The inertia forces, the weights, and the friction forces at the slider connections can be neglected when compared to the total deformation force of the tiebars and the thrust of the crosshead.
(3) The deformation effects of the mold and the mold platens are negligible.
(4) Coulomb friction is valid for the friction at pin joints.
(5) The friction coefficients are the same for all pin joints.

Due to assumption (1), the equilibrium equations of the toggle clamping system are constructed at the undeformed configuration of the toggle clamping system during real-mold clamping operation in this study.

Fig. 2 depicts a skeleton drawing for the lower half of the toggle clamping mechanism shown in Fig. 1 during real-mold clamping operation. The dashed lines denote the configuration when the moving platen is just in contact with the stationary platen. It is assumed that the toggle mechanism and the tiebars are not yet deformed in this configuration. After the contact, the toggle linkage is subjected to compressive force. Thus, besides the rigid body motion, there arises the compressive

deformation for the toggle linkage. It can be seen from the solid line shown in Fig. 2, the moving platen is at rest and the tailstock platen moves backward after the contact. The final position of real-mold clamping operation is achieved when the toggle is fully extended in a straight line. In this paper, the symbol (˜) denotes that the quantity in parentheses is in the state of the final position of mold clamping operation.

From Fig. 2, the geometry of the final position of the mold clamping operation, and the assumption of small deformation, we may have

$$L_2 \sin\alpha_C - L_1 \sin\beta_C = (L_2 - \delta_{BC}) \sin\alpha - (L_1 - \delta_{AB}) \sin\beta = d_A, \tag{1}$$

$$\begin{aligned} &L_4 \sin(\alpha_C + \gamma_C) + L_3 \sin\phi_C \\ &\quad = (L_{CF} - \delta_{CF}) \sin\alpha + L_4 \sin\gamma_C \cos\alpha + (L_3 - \delta_{DE}) \sin\phi = d_E, \end{aligned} \tag{2}$$

$$\tilde{\alpha} = -\tilde{\beta}, \tag{3}$$

$$L_{CF} = L_4 \cos\gamma_C, \tag{4}$$

$$\tan\gamma = \frac{L_4 \sin\gamma_C}{(L_{CF} - \delta_{CF})}, \tag{5}$$

$$\begin{aligned} S_C &= (L_1 - \delta_{AB}) \cos\beta - L_1 \cos\beta_C + (L_2 - \delta_{BC}) \cos\alpha - L_2 \cos\alpha_C \\ &= \bar{S}_C - \delta_{AB} \cos\beta - \delta_{BC} \cos\alpha, \end{aligned} \tag{6}$$

$$\bar{S}_C = L_1(\cos\beta - \cos\beta_C) + L_2(\cos\alpha - \cos\alpha_C), \tag{7}$$

$$\begin{aligned} U_E = {} & L_1 \cos\beta_C - (L_1 - \delta_{AB}) \cos\beta \\ & + (L_2 - L_{CF}) \cos\alpha_C - (L_2 - L_{CF} - \delta_{BF}) \cos\alpha \\ & + L_4 \sin\gamma_C(\sin\alpha_C - \sin\alpha) + L_3 \cos\phi_C - (L_3 - \delta_{DE}) \cos\phi, \end{aligned} \tag{8}$$

where $L_i$ ($i = 1$–4) and $L_{CF}$ are the distance between joints $A$ and $B$, $B$ and $C$, $D$ and $E$, $C$ and $D$, and $C$ and $F$, respectively, at the undeformed state of the mechanism, $S_C$ is the elongation of the tiebars; $\delta_{AB}$, $\delta_{BC}$ and $\delta_{DE}$ are the axial shortened length of links 1, 2 and 3, respectively, $\delta_{BF}$ and $\delta_{CF}$ are the shortened length of axial segments $BF$ and $CF$ of links 2, respectively, $U_E$ is the horizontal displacement of the crosshead. Due to assumption of small deformation, $\delta_{AB}$, $\delta_{BC}$, $\delta_{DE}$, $\delta_{BF}$ and $\delta_{CF}$ in Eqs. (1), (2), (5) and (8) are dropped in this study. Thus, one can obtain the values of $\tilde{\alpha}$, $\tilde{\beta}$, $\tilde{\phi}$ and $\tilde{\gamma}$ using Eqs. (1)–(5). Note that the deformations $\delta_{AB}$ and $\delta_{BC}$ are only considered in Eq. (6) in this study.

Let $F_{ij}$ shown in Fig. 3 represent the force exerted by all members $i$ on a single member $j$. The circles shown in Fig. 3 are called friction circles [3,5]. For the sake of clarity, the friction circles in Fig. 3 have been greatly exaggerated in magnitude. From Figs. 1 and 3, the free-body diagrams for each member and joint can be easily drawn (not shown), and the equations of equilibrium required for the real-mold clamping operation are given by

$$n_2 F_{12} = n_1 F_{21} = n_1 F_{61} = F_{16}, \tag{9}$$

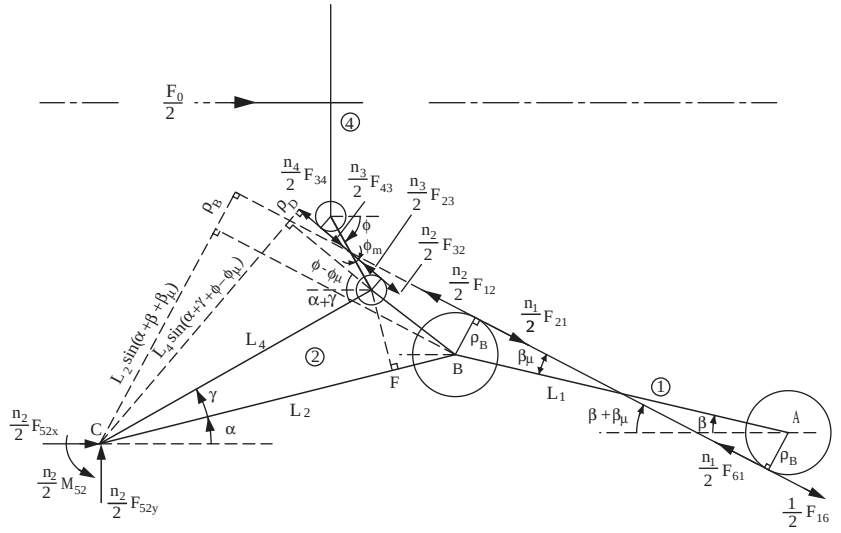


Fig. 3. Toggle linkage subjected to loading during real-mold clamping.

$$F_{cl} = F_{16}\cos(\beta + \beta_\mu), \tag{10}$$

$$n_4F_{34} = n_3F_{43} = n_3F_{23} = n_2F_{32}, \tag{11}$$

$$F_0 = n_4F_{34}\cos(\phi - \phi_\mu), \tag{12}$$

$$F_{52x} = F_{12}\cos(\beta + \beta_\mu) - F_{32}\cos(\phi - \phi_\mu), \tag{13}$$

$$F_{52y} = F_{32}\sin(\phi - \phi_\mu) - F_{12}\sin(\beta + \beta_\mu), \tag{14}$$

$$M_{52} = F_{32}[L_4\sin(\alpha + \gamma + \phi - \phi_\mu) + \rho_D] - F_{12}[L_2\sin(\alpha + \beta + \beta_\mu) + \rho_B]$$
$$= \rho_C\sqrt{F_{52x}^2 + F_{52y}^2} \geqslant 0, \tag{15}$$

$$F_c = n_2F_{52x}, \tag{16}$$

$$\beta_\mu = \sin^{-1}\left(\frac{2\rho_B}{L_1}\right), \qquad \phi_\mu = \sin^{-1}\left(\frac{2\rho_D}{L_3}\right), \tag{17}$$

$$\rho_B = \frac{\mu}{\sqrt{1+\mu^2}}r_B, \qquad \rho_C = \frac{\mu}{\sqrt{1+\mu^2}}r_C, \qquad \rho_D = \frac{\mu}{\sqrt{1+\mu^2}}r_D, \tag{18}$$

where $n_i$ ($i = 1$–$4$) are the number of member $i$. In Eq. (10), $F_{cl}$ is the clamping force shown in Fig. 1. In Eq. (12), $F_0$ is the thrust transmitted to the crosshead shown in Fig. 1. In Eq. (16), $F_c$ is the total tension of all tiebars (member 7). In Eq. (18), $\mu$ is the friction coefficient in all pin joints, $r_B$, $r_C$, and $r_D$ are the radiuses of pin joints $B$, $C$, and $D$, respectively, and $\rho_B$, $\rho_C$, and $\rho_D$ are the

corresponding friction radiuses, respectively. Note that the radius of joint $A$ is equal to the radius of joint $B$ and the radius of joint $E$ is equal to the radius of joint $D$ in this study. Moment $M_{52}$ in Eq. (15) must be nonnegative, because the rotation of links 2 is clockwise during the mold clamping operation.

From Eqs. (9) and (10), and Fig. 3, the compressive axial force in a single link 1 may be expressed as

$$F_{AB} = \frac{F_{cl}\cos\beta_\mu}{n_1\cos(\beta+\beta_\mu)}. \tag{19}$$

From Eqs. (9)–(12), and Fig. 3, the compressive axial force in the segments $BF$ and $CF$ of a single link 2 may be expressed as

$$F_{BF} = \frac{F_{cl}}{n_2}\frac{\cos(\alpha+\beta+\beta_\mu)}{\cos(\beta+\beta_\mu)}, \tag{20}$$

$$F_{CF} = F_{BF} - \frac{F_0\cos(\alpha+\phi-\phi_\mu)}{n_2\cos(\phi-\phi_\mu)}. \tag{21}$$

From Eqs. (19)–(21), $\delta_{AB}$ and $\delta_{BC}$, the axial shortened length of links 1 and 2 defined in Eq. (6), may be expressed by

$$\delta_{AB} = \frac{F_{AB}L_1}{A_1E_1}, \tag{22}$$

$$\delta_{BC} = \frac{F_{CF}L_4\cos\gamma}{A_2E_2} + \frac{F_{BF}(L_2-L_4\cos\gamma)}{A_2E_2}, \tag{23}$$

where $A_i$ and $E_i$ $(i=1,2)$ are the cross-sectional area and Young's modulus of links 1 and 2, respectively.

The elongation of the tiebars, $S_C$, given in Eq. (6) may be expressed by

$$S_C = \frac{F_cL_c}{n_cA_cE_c}, \tag{24}$$

where $F_c$ is the total tension of all tiebars given in Eq. (16), $n_c$ is the number of tiebar, $A_c$ and $E_c$ are the cross-sectional area and Young's modulus of tie bar, respectively.

Substituting Eqs. (22)–(24) into Eq. (6), one may obtain

$$\frac{F_cL_c}{n_cA_cE_c} + \frac{F_{AB}L_1}{A_1E_1}\cos\beta + \left[\frac{F_{CF}L_4\cos\gamma}{A_2E_2} + \frac{F_{BF}(L_2-L_4\cos\gamma)}{A_2E_2}\right]\cos\alpha = \bar{S}_C. \tag{25}$$

Using Eqs. (13)–(15), one may obtain

$$aF_{32}^2 - 2bF_{12}F_{32} + cF_{12}^2 = 0, \tag{26}$$

where

$$a = k_1^2 - k_3, \qquad b = k_1k_2 - k_3k_4, \qquad c = k_2^2 - k_3,$$
$$k_1 = L_4\sin(\alpha+\gamma+\phi-\phi_\mu) + \rho_D, \qquad k_2 = L_2\sin(\alpha+\beta+\beta_\mu) + \rho_B,$$
$$k_3 = \rho_C^2, \qquad k_4 = \cos(\beta+\beta_\mu-\phi+\phi_\mu). \tag{27}$$

From Eq. (26) and the inequality $M_{52} \geqslant 0$ given in Eq. (15), one may obtain

$$\frac{F_{12}}{F_{32}} = \frac{a}{b + \sqrt{b^2 - ac}}. \tag{28}$$

From Eqs. (9)–(12) and (28), one may obtain the mechanical advantage of the five-point double toggle mechanism as

$$\frac{F_{cl}}{F_0} = \frac{a}{b + \sqrt{b^2 - ac}} \frac{\cos(\beta + \beta_\mu)}{\cos(\phi - \phi_\mu)}. \tag{29}$$

From Eqs. (9)–(13) and (16), one may obtain

$$F_c + F_0 = F_{cl}. \tag{30}$$

Substituting Eqs. (19)–(21) into Eq. (25), we can obtain the relation among the total deformational force of the tiebars $F_c$, the clamping force $F_{cl}$, and the necessary thrust of the crosshead $F_0$ from Eqs. (25), (29), and (30).

For a specified final clamping force, the final total deformational force of the tiebars and the thrust of the crosshead can be obtained from Eqs. (29) and (30). Then, the final deformations for links 1, 2 and tiebars can be calculated from Eqs. (19)–(24). Then, using Eqs. (1), (2), (6) and (7), we can determine the values of $\alpha_C$, $\beta_C$, and $\phi_C$ required at the beginning of the real-mold clamping operation.

In order to verify the accuracy of the present study and estimate the friction coefficient at pin joints, the experimental data from a fully electric injection molding machine SM-55 with clamping capacity 55 metric tons, being developed by Chen Hsong Machinery Taiwan Co., Ltd., are compared in this study. The SM-55 with a clamping servo electric motor connected with a motion controller (motion card) via a CPU bus, from Mitsubishi Electric Co., Ltd., can output the recording curves of the measured values of the current, the swiveling speed, and the pulse versus time during mold clamping operation. The servo electric motor is used to actuate the toggle clamping system in the machine. The motor can actuate the screw shaft of ballscrew to rotate by torque for driving the nut of ballscrew to move in a straight line. The thrust $F_0$ is transmitted to the crosshead locked on the nut of ballscrew by the driver gear, the synchronous belt, and the driven gear fastened on the screw shaft of ballscrew. An absolute optical position encoder is equipped on the servo electric motor, which generates $N_s$ pulses per revolution of the motor shaft. The zero value of the pulse from the encoder is set at the final clamping position. Let $N_c$ denote the number of pulses measured from the initial contact position of the moving mold and the stationary mold to the final clamping position. The corresponding displacement of the crosshead may be expressed as

$$\tilde{U}_E = \frac{N_c}{N_s} R\ell, \tag{31}$$

where $R$ is the velocity ratio of the driven gear to the driver gear, $\ell$ is the lead of the ballscrew. Due to assumption of small deformation, $\delta_{AB}$, $\delta_{BF}$ and $\delta_{DE}$ in Eq. (8) are dropped in this study. Using Eqs. (1), (2), (8) and (31), one may obtain the values of $\alpha_C$, $\beta_C$, and $\phi_C$.

Let $T_m$ denote the motor torque. The relation between the torque $T_m$ and the thrust $F_0$ is given by

$$T_m = \frac{F_0 \mathrm{R}\ell}{2\pi\eta}, \tag{32}$$

where $\eta$ is the mechanical efficiency of the drive system. The mechanical efficiency of the synchronous belt is about 96–98%, and that of the ballscrew converting rotary motion to linear motion is about 85–95% [6]. Note that the motor torque required for deceleration operation [6] is assumed to be negligible here.

## 3. Example

A practical example of toggle mechanism of a fully electric injection molding machine SM-55, being developed by Chen Hsong Machinery Taiwan Co., Ltd., is studied. The geometric properties are as follows: $L_1 = 231$ mm, $A_1 \approx 2184$ mm$^2$, $n_1 = 6$ for links 1; $L_2 = 164$ mm, $L_4 = 133.17$ mm, $\gamma_C = 28.49°$, $A_2 \approx 3276$ mm$^2$, $n_2 = 4$ for links 2; $L_3 = 70.27$ mm, $n_3 = 2$ for crosshead links; $L_c \approx 1250$ mm, $A_c \approx 2827$ mm$^2$, $n_c = 4$ for the tiebars; $d_A = 5$ mm, $d_E = 135$ mm, $r_B = 22.5$ mm, $r_C$=22.5 mm, $r_D$=15.0 mm. Young's modulus of the toggle links made of ductile irons is 17 593 kgf/mm$^2$, and Young's modulus of the tiebars made of Cr–Mo steels is 20 800 kgf/mm$^2$. The specifications related to the derive system are as follows: the rated torque of the servo electric motor with the rated swiveling speed 2000 rpm is 2440 kgf mm; the velocity ratio $R = 30/42$; the lead $\ell = 20$ mm; $N_s = 16384$ pulse per revolution. In the example, $\tilde{\alpha} = 0.7253°$, $\tilde{\beta} = -0.7253°$, and $\tilde{\phi} = 84.9825°$, when the final clamping position is achieved.

This example is divided into two parts. In the first part, the friction effect of pin joints is investigated. In the second part, the friction coefficient for the example is estimated.

### 3.1. Friction effect of pin joints

To investigate the influence of the friction coefficient on the mechanical advantage and the necessary thrust of the crosshead, the final total deformational force of the tiebars $\tilde{F}_c = 55\,000$ kgf,

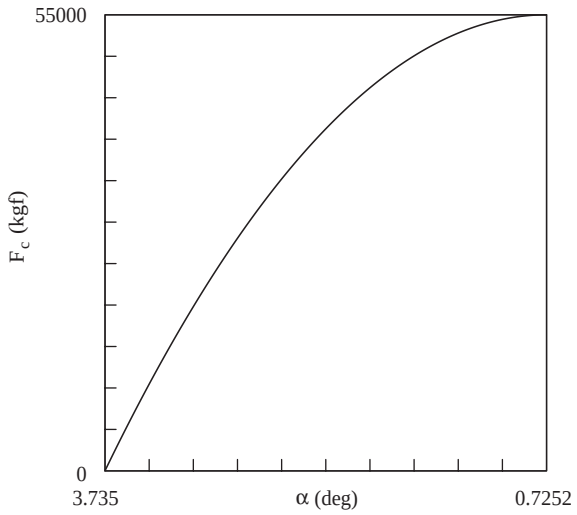


Fig. 4. Total deformational force of the tiebars versus angle α.

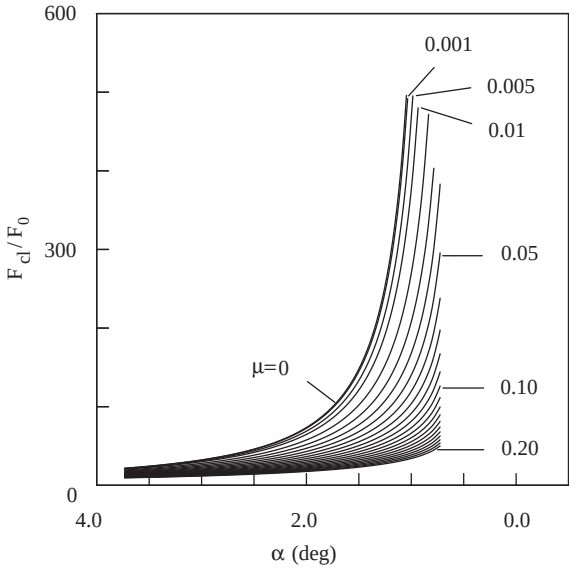


Fig. 5. Mechanical advantage versus angle α.

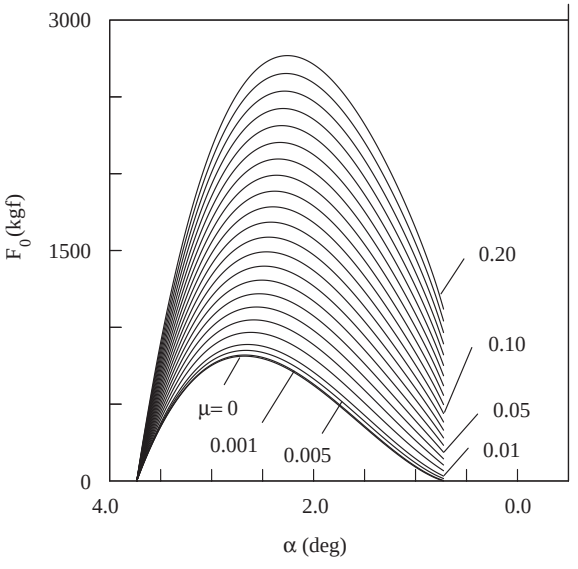


Fig. 6. Thrust applied to the crosshead versus angle α.

and different values of the friction coefficient $\mu$ were used. The value of $\alpha_C$ corresponding to $\tilde{F}_c =$ 55 000 kgf is 3.735°. The values of $\tilde{S}_C$ and $\tilde{U}_E$ are 0.2923 and 26.08 mm. Fig. 4 shows the graph of the total deformation force of the tiebars versus angle α. Fig. 5 shows the curves of mechanical advantage versus angle α under the various friction coefficients. Fig. 6 shows the variation of the

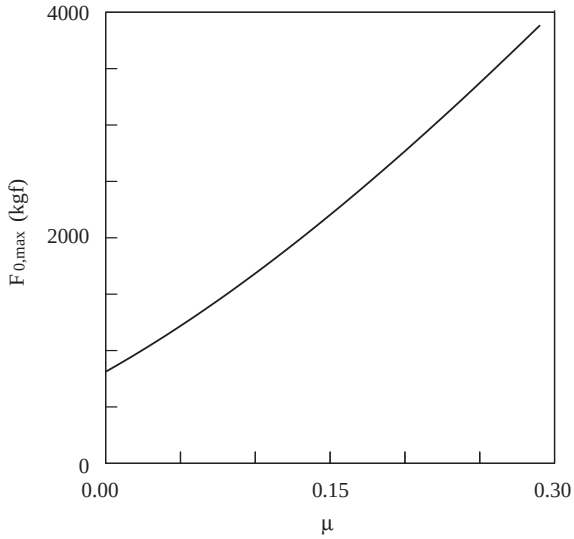


Fig. 7. Maximum thrust applied to the crosshead versus the friction coefficient.

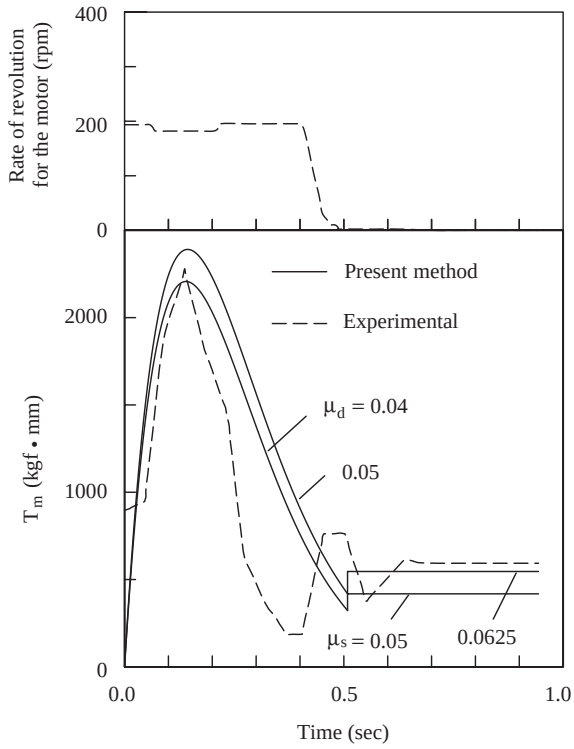


Fig. 8. Motor torques versus time from the first experiment and the present simulation with $\eta = 80\%$.

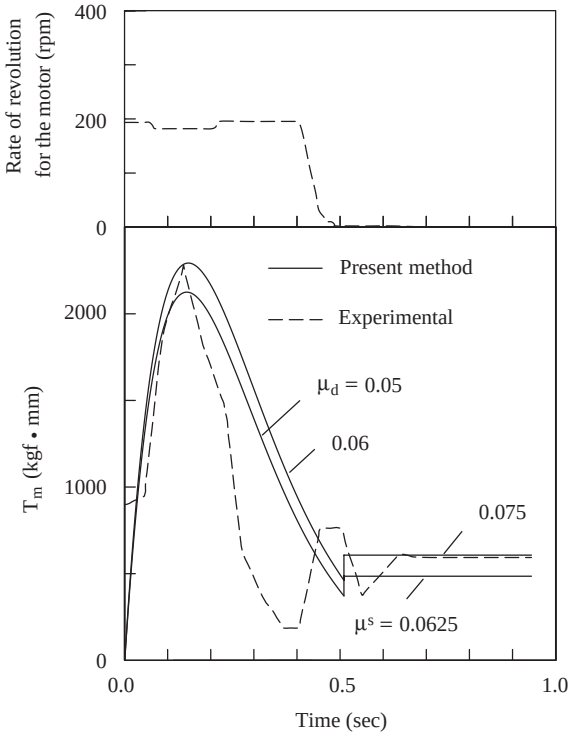


Fig. 9. Motor torques versus time from the first experiment and the present simulation with $\eta = 90\%$.

necessary thrust of the crosshead with the angle $\alpha$ for several friction coefficients. It can be seen from Figs. 4–6 that the necessary thrust of the crosshead increases rapidly after the occurrence of real-mold clamping, and decreases rapidly after reaching the maximum value. The maximum thrust is occurred neither at the initial position of real-mold clamping nor at the final position. The increase rate of the necessary thrust is consistent with that of the mechanical advantage and that of deformation force of tiebars. The necessary input force for selecting the size of the clamping cylinder or servo electric motor should be directly based on the necessary thrust of the crosshead, rather than the mechanical advantage. The relation between the maximum thrust of the crosshead $F_{0,\max}$ and the friction coefficient $\mu$ is shown in Fig. 7. In the absence of hinge friction, the maximum thrust of the crosshead is 808.78 kgf. The maximum thrusts of the crosshead are 884.42, 1212.37, 1674.88, and 2408.22 kgf for friction coefficients 0.01, 0.05, 0.10, and 0.17, respectively. Thus, the effect of the friction coefficient on the thrust of the crosshead is not negligible, when its value is larger than 0.05. Note that the thrust of the crosshead is not zero at the final clamping position in practice.

### *3.2. Estimation of the friction coefficient*

The SM-55 with a clamping servo electric motor and a motion control card, from Mitsubishi Electric Co., Ltd., can output the recording curves of the measured values of the current, the swiveling speed, and the pulse versus time during mold clamping operation. To estimate the friction coefficient

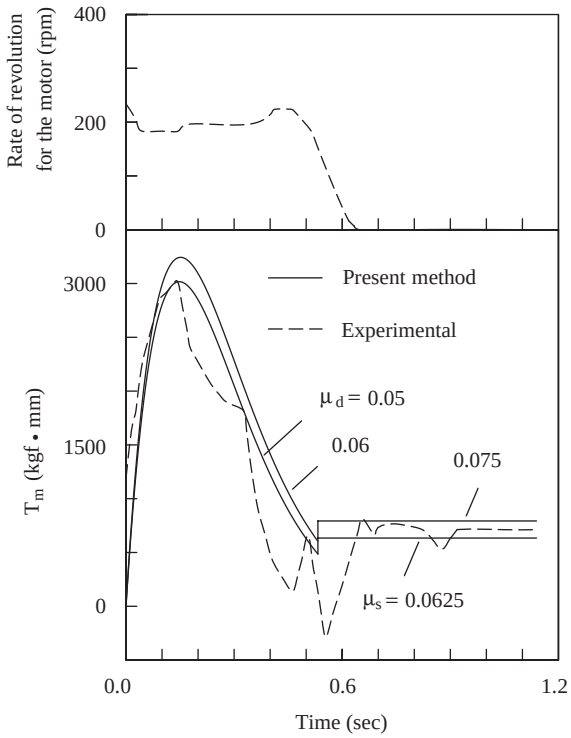


Fig. 10. Motor torques versus time from the second experiment and the present simulation with $\eta = 80\%$.

of pin joints, two experimental motor torques during real-mold clamping are compared with those obtained from the present model. The experimental values of the motor torques are obtained based on the measured value of the current. In the present simulation, the mechanical efficiency $\eta$ of the derive system used in Eq. (32) for calculating motor torque is assumed to be 80% and 90%. For the first experiment, the rate of revolution for the motor during real-mold clamping is shown in the upper part of Fig. 8 and the value of $N_c$ is 27 790 pulse. The value 200 rpm is used here for simulation. The comparison between the motor torques from the experiment and the present simulation is shown in Figs. 8 and 9. In Figs. 8 and 9, the kinetic friction coefficients $\mu_d = 0.04$, 0.05 and 0.05, 0.06 and the mechanical efficiency of the drive system $\eta = 80\%$ and 90%, respectively, are used during real-mold clamping for simulation. The static friction coefficient $\mu_s = 1.25\mu_d$ is used after the final clamping position is achieved. For the second experiment, the rate of revolution is shown in the upper part of Fig. 10 and the value of $N_c$ is 29 110 pulse. The value 200 rpm is used here for simulation. The comparison between the motor torques from the experiment and the present simulation is shown in Figs. 10 and 11. In Figs. 10 and 11, the kinetic friction coefficients $\mu_d = 0.05$, 0.06 and 0.06, 0.07 and the mechanical efficiency of the drive system $\eta = 80\%$ and 90%, respectively, are used during real-mold clamping for simulation. The static friction coefficient $\mu_s = 1.25\mu_d$ is used after the final clamping position is achieved. From Figs. 8–11, we might consider the kinetic friction coefficients to be 0.05 and 0.07 corresponding to the mechanical efficiency of the drive system $\eta = 80\%$ and 90%, respectively, in design. It can be seen from Figs. 8–11 that the agreement between the experimental

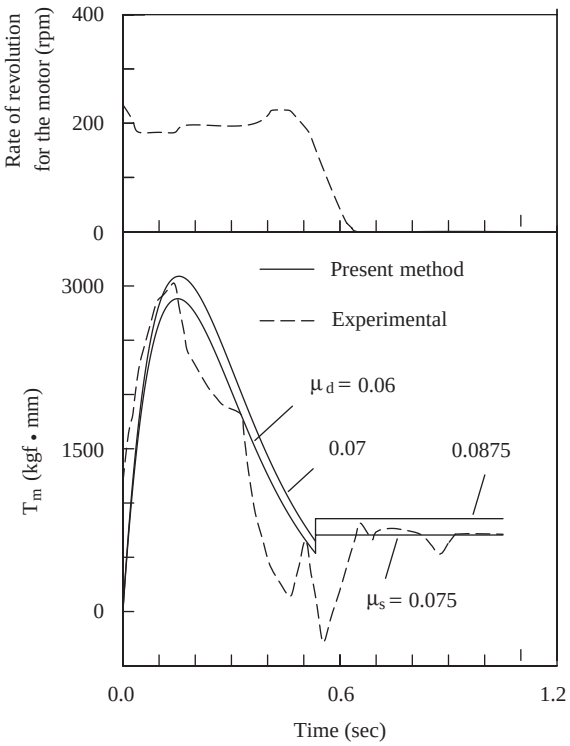


Fig. 11. Motor torques versus time from the second experiment and the present simulation with $\eta = 90\%$.

results and those obtain by the present study is qualitatively good, each set showing rapid increase of motor torque after the occurrence of real-mold clamping, and then rapid decrease after reaching its peak. However, quantitatively there are considerable differences. The motor torque before real-mold clamping in the experimental curve seems to be relatively large. This torque maybe arise from that the weight of the moving platen and mold is not directly supported by the support blocks (or rollers) of the moving platen on the steel brand fixed on the frame, which causes the lateral deformation of the tiebars suffering from the lateral (vertical) loading. This torque might be greatly reduced by properly adjusting the support block to take the much greater part of the weight of the moving platen and mold. The sharp decrease of motor torque after reaching its peak for the experimental curves may be attributed at least in part to the snapping phenomenon under dynamic load condition. The discrepancy between the results of the present method and the experimental results may be much alleviated if the inertia effects are considered in the present method.

## 4. Conclusion

An analytical formulation for the necessary thrust of the crosshead on the five-point double-toggle clamping mechanism during real-mold clamping operation is proposed using the Coulomb friction. It has been shown that the friction at pin joints should not be neglected for the real-mold clamping

operation. The kinetic coefficient of friction at pin joints is estimated by adjusting the required motor torque curve for real-mold clamping using different values of coefficient of friction and mechanical efficiency for the present study to fit the experimental data. The agreement between the motor torques obtained by the experiments and those obtained by the present method is qualitatively good. It seems that the inertia effects are not negligible during real-mold clamping operation for reliable analysis.

## Acknowledgements

The authors are grateful to Chen Hsong Machinery Taiwan Co., Ltd., for providing the recording curves for the measured values of the current, the swiveling speed, and the pulse. The authors would like to acknowledge the constructive and thoughtful comments of the referees.

## References

[1] Johannaber F. Injection molding machines. New York: Hanser; 1994.
[2] Smith A. How to choose a plastics injection moulding machine. Bristol: AMI Business Publishing; 1995.
[3] Burton P. Kinematics and dynamics of planner machinery. Englewood Cliffs, NJ: Prentice-Hall; 1979.
[4] Spotts MF. Design of machine elements. Englewood Cliffs, NJ: Prentice-Hall; 1985.
[5] Wilson CE, Sadler JP, Michels WJ. Kinematics and dynamics of machinery. New York: Harper and Row; 1983.
[6] HIWIN Technologies Corp. Catalog of HIWIN ballscrews, Taichung, 1992.